

# Soap Film Thickness Imaging by Infrared Methods

Ryan Mackey

Graduate Aeronautical Laboratories

California Institute of Technology

December 1996

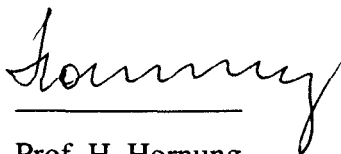
Submitted for Partial Satisfaction  
of the Requirements for the Degree of Engineer  
Aeronautics Option

1997


Thesis Committee:



Prof. M. Gharib



Prof. H. Hornung



Prof. A. Leonard



## TABLE OF CONTENTS

|                                     |    |
|-------------------------------------|----|
| 1. Abstract . . . . .               | 4  |
| 2. Introduction . . . . .           | 5  |
| 3. Film Properties . . . . .        | 6  |
| 4. Infrared Theory . . . . .        | 9  |
| 5. Experimental Procedure . . . . . | 13 |
| 6. Results . . . . .                | 14 |
| 7. Discussion . . . . .             | 17 |
| 8. Conclusions . . . . .            | 18 |
| 9. Bibliography . . . . .           | 19 |

## LIST OF FIGURES

|  |    |
|--|----|
| 1. Thin-film interference problem schematic . . . . .                          | 20 |
| 2. Blackbody spectrum at liquid nitrogen temperature . . . . .                 | 20 |
| 3. Blackbody spectrum at room temperature . . . . .                            | 21 |
| 4. Simplified experimental setup . . . . .                                     | 21 |
| 5. Experimental setup – schematic, top view . . . . .                          | 22 |
| 6. Detail – infrared camera . . . . .  | 23 |
| 7. Experimental setup – schematic, front view . . . . .                        | 24 |
| 8. Detail – view along the camera . . . . .                                    | 25 |
| 9. Detail – region to be imaged . . . . .                                      | 25 |
| 10. Detail – soap solution reservoir. . . . .                                  | 25 |
| 11. Detail – calibration frame in place . . . . .                              | 25 |
| 12. Calibration data – visible light photograph . . . . .                      | 26 |
| 13. Calibration data – infrared photograph . . . . .                           | 26 |
| 14. Processed calibration data . . . . .                                       | 27 |
| 15. Raw image – Film tunnel flow undisturbed . . . . .                         | 28 |
| 16. Raw image – Film tunnel flow with separated boundary layers . . . . .      | 28 |
| 17. Raw image – Cylinder inserted at wall . . . . .                            | 29 |
| 18. Raw image – Larger picture: cylinder inserted at wall . . . . .            | 29 |
| 19. Detail – Grid . . . . .  | 30 |
| 20. Raw image – Flow behind the grid . . . . .                                 | 30 |
| 21. Processed image – Film tunnel flow undisturbed . . . . .                   | 31 |
| 22. Processed image – Film tunnel flow with separated boundary layers. . . . . | 32 |
| 23. Processed image – Cylinder inserted at wall . . . . .                      | 33 |
| 24. Processed image – Flow behind the grid . . . . .                           | 34 |
| 25. Comparison – Cylinder inserted at wall, two consecutive images . . . . .   | 35 |

## ACKNOWLEDGEMENTS

This work was conducted under the Powell Research Fund, supervised by Prof. M. Gharib.

The author would like to recognize the individuals who provided the various infrared imagers used in this research. They are Dr. E. Trinh of the Jet Propulsion Laboratories, Section 354; Mr. G. Siebes of the Jet Propulsion Laboratories, Section 353; and Prof. W. Knauss of the California Institute of Technology. I would particularly like to thank Prof. M. Beizaie of the University of California at San Diego for his expertise in constructing the film tunnel used for this research. I would also like to thank Mr. V. Daggumati of the Jet Propulsion Laboratories, Section 395 for technical assistance during image processing.

## ABSTRACT

A new method of studying soap film flows is introduced and discussed from several viewpoints. Using a commercial infrared camera and a cold background as an infrared light source, one can recover non-intrusively a measurement of the film thickness distribution. Once the thickness is known it is easy to compute the two-dimensional pressure in the film, allowing one to compute other film properties as well.

Blackbody and infrared detector theory are covered in brief and a simple theory of operation is introduced to explain the connection between emissivity and thickness. This theory is demonstrated to behave similarly to the physical system, predicting detected temperature values as a function of thickness of the same approximate magnitude as observed, but is too simple to provide a perfect match. An empirical calibration routine is demonstrated allowing one to calculate the film thickness to a high degree of precision.

The infrared method is applied to a number of familiar test problems as a demonstration. A gravity driven soap film tunnel has been constructed, and infrared images of the film surface are provided for unobstructed flow, separated flow past a cylinder held at one wall, and turbulent flow through a grid. These images are presented in raw and processed formats and the phenomena observed are discussed.

## INTRODUCTION

This work is intended to provide experimenters with a simple method for gathering global, instantaneous, non-invasive measurement of thickness in liquid film flows. Using this method, it is possible to obtain quantitative data about the film where only qualitative data (such as that given by visible-light photography) or data at a single point (e.g., LDV measurement) was available before. This allows a variety of studies to be conducted, in particular comparisons of two-dimensional flow phenomena with corresponding three-dimensional cases, and provides a method to validate two-dimensional computations. By providing a background of suitably different temperature from the laboratory, the thickness of a soap film can be quickly extrapolated from thermal images. The amount of thermal energy transmitted through the film from the background and the amount reflected from the laboratory, and the total energy can be measured accurately using an infrared camera.

The method has a number of facets that must be addressed, namely the geometry of the film flow, the background and laboratory conditions, the infrared imager itself, and the calibration of the method for an individual setup. Presented here is a setup and calibration procedure that works satisfactorily as well as a rough working theory of the phenomenon as a whole. This paper will cover the aspects of film theory, infrared theory, the apparatus used in these experiments and suggested improvements, calibration methods and data, and raw and processed images of typical film experiments as a benchmark.

Soap films have long been of interest to experimenters, primarily because of the two-dimensionality of the film. Studies have been made of the flow within a fixed frame, a sheet of moving fluid in a sort of film tunnel, bubbles and spherical flows, and so on. Because the film can be considered as truly two-dimensional, many of these problems can be observed in no other way save computer simulation.

The problems we will revisit involve a film tunnel, similar to that presented by Gharib and Derango (1989), where a sheet of film is pulled over an open frame at constant speed and continually replenished. Our tunnel is vertical and relies on gravity to provide motion. It is a simple matter to introduce obstacles to this flow or change the configuration of the frame in order to study cavity flow, nozzles, grid turbulence, etc., in two dimensions. A careful study of these problems allows one to verify solutions to the Reynolds film equation and compare to any computer prediction.

Unfortunately, films present their own difficulties. Nearly all previous studies rely on photographs taken in visible light, which produces interference patterns depending on the film thickness. This reveals the magnitude of the thickness gradient and so doing exposes the character of the flow, but such photographs are qualitative only. In order to calculate the thickness from visible photographs more must be known about the film, namely the direction of the gradient as well as a known reference point, which in general cannot be determined.

There have been serious efforts to apply laser doppler velocimetry (LDV) to soap films, as well as strain gages and similar instruments. While such measurements can be effective, there are inherent

problems. First, film properties are affected by any intrusion, including the introduction of dye or marker particles. Second, the majority of these methods only reveal flow properties at a single point. It is highly desirable to employ a method that is both non-intrusive and global for a proper quantitative study.

## FILM PROPERTIES

In general, a soap film is a sheet of water with a small concentration of a surfactant. The surfactant “soap molecule” has a physical length as well as both hydrophobic and hydrophilic ends. Because of this, the vast majority of the surfactant molecules flock to the surface of the water, where they form the skin of the film.

For our experiments, the impurity is roughly 1%. The film averages between 3.6  $\mu\text{m}$  and 5.3  $\mu\text{m}$  in the film tunnel, and reaches from 0.1  $\mu\text{m}$  to 7  $\mu\text{m}$  or more during calibration. The tunnel speed is about 30 cm/s, much slower than the typical sound speed of  $\sim 5$  m/s, though this method can be applied to much faster studies as well.

The following derivation highlights the importance of film thickness, as first presented by Couder et al. (1989) and Chomaz et al. (1990). Throughout this summary the following notation will be used:

- (1)
- $h$  = thickness
  - $C$  = bulk concentration of surfactant
  - $\Gamma$  = surface concentration of surfactant
  - $\mu$  = surface viscosity
  - $n$  = index of refraction
  - $T$  = temperature reported by the infrared imager
  - $T_1$  = laboratory temperature
  - $T_{bg}$  = infrared background temperature
  - $T_d$  = detector temperature
  - $\sigma$  = surface tension
  - $\rho$  = density
  - $K$  = surfactant absorption

Quantities subscripted as  $X_0$  refer to the constant term of quantity  $X$ , whereas  $X_1$  refers to the variable component.

By manipulating the film equations, we shall find a clear relationship between the thickness and the pressure, or rather the variation in surface tension, in the film. Because of this, it is highly useful to know the thickness of the film.

There are two components of elasticity in the film. They are the Marangoni elasticity, which is the contribution from the surface; and the Gibbs elasticity, which comes from the interior of the film. For reasonably slow processes, we can ignore the Gibbs elasticity. We will also assume that there is no differential transport in the interior of the film. Having done so, we can write the Reynolds equation as follows:

$$(2) \quad \rho h \frac{D\bar{u}}{Dt} = 2\nabla\sigma + h\mu\nabla^2\bar{u}$$

We are also given these conservation equations, the first for thickness, and the second for film concentration:

$$(3) \quad \frac{Dh}{Dt} = -h\bar{\nabla} \cdot \bar{u}$$

$$(4) \quad \frac{D\Gamma_1}{Dt} = -\Gamma_1\bar{\nabla} \cdot \bar{u} - \frac{1}{\tau_G} \left( \Gamma_1 - \frac{C_0 h K}{h + 2K} \right)$$

Here  $\tau_G$  is the Gibbs time-scale, which we can safely assume to be much larger than one second. The time-scale in our experiments is no greater than one-half second, so we can ignore the last term of equation (4). Now we rewrite the Reynolds equation in non-dimensional format, and arrive at the following system:

$$(5) \quad \frac{D\bar{u}}{Dt} = -\frac{1}{M^2} \frac{\nabla\Gamma_1}{h} + \frac{1}{Re} \nabla^2\bar{u}$$

$$(6) \quad \frac{D\Gamma_1}{Dt} = -\Gamma_1\bar{\nabla} \cdot \bar{u}$$

$$(7) \quad \frac{Dh}{Dt} = -h\bar{\nabla} \cdot \bar{u}$$

Here we have introduced the familiar definitions:



$$(8) \quad \text{Re} = \frac{UL}{\nu}$$

$$(9) \quad \text{M} = \frac{U}{v_{\text{LF}}}$$

The sound speed is not needed here due to the slow nature ( $v \sim 30$  cm/s or less) of our studies, but in general  $v_{\text{LF}}$  is on the order of 5 m/s.

Since we assume slow fluid flow, we can expand asymptotically using  $\text{M}^2$  as a small parameter.

$$\text{Zero Order:} \quad (10) \quad \Gamma_{i_0} = h_0 = 1$$

$$\text{First Order:} \quad (11) \quad \vec{\nabla} \cdot \vec{u}_0 = 0$$

$$\text{Second Order:} \quad (12) \quad \frac{\partial h_1}{\partial t} + (\vec{u}_0 \cdot \vec{\nabla})h_1 = \frac{\partial \Gamma_1}{\partial t} + (\vec{u}_0 \cdot \vec{\nabla})\Gamma_1$$

From (12) we see that the thickness is an advected scalar following the concentration  $\Gamma_1$ . Furthermore, if we assume an unsaturated concentration, then we can apply the Gibbs absorption law:

$$(13) \quad \Gamma_1 = \text{KC}_1$$

The surface molecules then obey the perfect gas law, and we are left with the following:

$$(14) \quad P = \frac{nRT}{A} = \Gamma_1 RT_f$$

Therefore, given the thickness, we know the concentration, and therefore the pressure, except for an arbitrary constant.

## INFRARED THEORY

Most film flow details can be seen qualitatively using the interference of visible light. If a white light source is used, this interference produces the familiar bands of color. If the light source is monochromatic, interference produces regular dark and light bands on the film.

Consider the simple problem illustrated in Figure 1. Let the film have properties as before, and also suppose:

$$(15) \quad \begin{aligned} \lambda &= \text{wavelength of monochromatic light} \\ \theta &= \text{incident angle} \\ I_0 &= \text{intensity of incident light} \\ I_R &= \text{intensity of reflected light} \\ I_T &= \text{intensity of transmitted light} \end{aligned}$$

The difference in pathlength of the two beams determines whether we will have constructive or destructive interference. This pathlength depends on the thickness, the angle of incidence, and the index of refraction. The solution to this problem is well understood:

$$(16) \quad \frac{I_R}{I_0} = \sin^2\left(\frac{2\pi nh}{\lambda} \cos\theta\right) \quad \frac{I_T}{I_0} = \cos^2\left(\frac{2\pi nh}{\lambda} \cos\theta\right)$$

Define the emittance of the film as follows:

$$(17) \quad \epsilon_f = 1 - \frac{I_T}{I_0}$$

$\epsilon_f$  is the fraction of radiation coming from the film that is not attributable to the background, i.e., the fraction reflected from the laboratory as well as any light generated by the film itself. This is not an important distinction for visible light but is relevant when infrared light is considered, since all objects radiate appreciably in the infrared. However, this is a minor concern, and to avoid conflict we may assume that the film is at the same temperature as the laboratory.

More importantly, we now specify that any film flow we observe should be as flat as possible. This is necessary if the incident angle  $\theta$  is to be constant. If this is not the case, some method of computing  $\theta$  for any point on the film must be found.

From equation (16), increasing thickness results in a sinusoidal reflected intensity, giving rise to the alternating light and dark fringes visible under monochromatic light. This effect can be used to see small changes in the thickness with great success. However, we almost never know the order of any given fringe, so we cannot determine the thickness itself.

Suppose instead, however, that the wavelength of the incident light is so large that we never reach the first fringe. We are then restricted to the monotonically increasing part of the sine curve, there is no ambiguity, and we can determine uniquely the thickness from the reflected or the transmitted intensity. For a typical soap film, the maximum thickness is on the order of a few microns, requiring a wavelength in the tens of microns. Such a wavelength, in the middle or far infrared, can be produced using a blackbody as a source of illumination.

Any blackbody at a given temperature  $T$  produces an emission spectrum according to the familiar Planck's Radiation Formula:

$$(18) \quad E_{\lambda} = \frac{c_1 \lambda^{-5}}{e^{c_2/\lambda T} - 1}$$

$$c_1 = 3.74 \times 10^{10} \mu\text{W} \mu\text{m}^4 / \text{cm}^2 \quad c_2 = 14380 \mu\text{mK}$$

By differentiating, we can show that the peak intensity occurs at roughly the following wavelength:

$$(19) \quad \frac{c_2}{\lambda_{\text{peak}} T} \approx 5$$

For our experiment, we require a wavelength on the order of 15  $\mu\text{m}$  or greater, corresponding to a blackbody temperature of no greater than 190 K. As will be demonstrated later, the background should be as cold as possible for best accuracy. For our experiments, the blackbody is cooled to liquid nitrogen temperatures, roughly 77K. The other relevant temperature is that of the laboratory, at about 303 K. Figures 2 and 3 illustrate these two spectra.

All infrared cameras operate by measuring the amount of energy received by the detector from a given solid angle of space over a fixed interval of time. This measurement is then used to estimate the temperature of the object in view. Consider the simplified setup in Figure 4. The operating concept is as follows: The camera reports a temperature based on the total energy received from the film and from the background behind the film. Both the film and the background emit energy via blackbody radiation with the bulk of the energy in the infrared. Even though the temperatures of the background and the film are fixed, the camera will gather different amounts of energy depending on the intensity reflected by the film, which depends on the film thickness. This results in a range of temperatures being reported by the camera.

If we can relate the reported temperature to the energy gathered by the camera, we can use the interference relations to compute the film thickness from the temperature.

The total energy output is related to the temperature by the Stefan-Boltzmann law:

$$(20) \quad E = \epsilon \sigma T^4$$

Here,  $\epsilon$  is the emittance of the object and  $\sigma$  is the Stefan-Boltzmann coefficient. We will replace  $\sigma$  by the more general constant  $A$  in order to account for other, highly variable factors, such as geometry, camera response, software corrections, and so on. Since the same factors apply to all objects in the system, this will divide out of the equations.

The net energy received by the detector is equal to the sum of: the amount given off by the background that passes through the film, the amount given off by the laboratory reflected from the film, and minus the amount radiated by the detector itself. Write this as the following:

$$(21) \quad E = A \left[ (1 - \epsilon_f) T_{bg}^4 + \epsilon_f T_f^4 - T_d^4 \right]$$

Assuming a perfectly calibrated camera, the detector translates this energy into a temperature measurement by the inverse relation:

$$(22) \quad E = AT^4$$

We can disregard the detector temperature in (21) because its effects are removed by the camera software as well. Combining, we are left with the relation:

$$(23) \quad T^4 = (1 - \epsilon_f) T_{bg}^4 + \epsilon_f T_f^4$$

Manipulating this, we see:

$$(24) \quad \epsilon_f = \frac{T^4 - T_{bg}^4}{T_f^4 - T_{bg}^4}$$

Let us now substitute (17) for  $\epsilon_f$  in (24). Define the peak wavelength for the background temperature as follows:

$$(25) \quad \lambda = \frac{14380 \mu\text{mK}}{5 \cdot T}$$

Therefore, the temperature output by the camera follows:

$$(26) \quad \sin^2\left(\frac{2\pi nh}{\lambda}\right) = \epsilon_f = \frac{T^4 - T_{bg}^4}{T_f^4 - T_{bg}^4}$$

This gives us the relation between temperature and thickness. The effect of background temperature on the measurement is now clear as well. It is desirable to make  $T_{bg}$  as small as possible in order to reduce or remove the background term and to increase the possible range of  $T$ . In the limit of  $T_{bg} = 0$ , we are left with the simple relation

$$(27) \quad \frac{T}{T_f} = \sqrt{\sin\left(\frac{2\pi nh}{\lambda_f}\right)}$$

In practice, the lower bound of  $T_{bg}$  will be set by the limitations of the camera used as well as other practical concerns.

These equations are oversimplified, but at least provide some physical justification for the phenomenon observed. The following assumptions were necessary for this derivation:

1. The blackbody spectra were assumed to be monochromatic using the peak wavelength from the Planck formula. We do not account for the very broad spectra actually present, which will tend to blur the sine relation between reflectivity and thickness. In practice we will likely encounter a more linear increase.
2. The camera response is very complex, and depends on numerous factors, including geometry, detector temperature, optics, filters, detector type and composition. This response is certain to be different for different cameras and also varies over different parts of the infrared spectrum.
3. Most importantly, radiation reflected from the laboratory is very poorly understood with respect to geometry, and is not handled correctly here. The emittance  $\epsilon_f$  and wavelength  $\lambda$  also depend on temperature, which we have ignored. However, the contribution of the laboratory is smaller than one would expect. Since the camera axis is normal to the film, any light reflected into the camera is at a very high angle of incidence, namely coming from the camera itself. The camera aperture does not emit radiation at the laboratory temperature, but rather at the much colder detector temperature.

4. We do not know how much energy is emitted by the film itself, although we suspect this contribution is very small. This experiment was performed a number of times using a heated soap solution in an attempt to create a heated film, hampered by the unfavorable response of a soap film to temperature changes. No measurable difference in reported temperature was observed.

For these reasons, it is necessary to undergo a calibration routine to avoid these problems. Such a routine will be discussed in the following section. We should not expect complete agreement between equation (26) and the calibration routine, but the character of the relation should be similar.

## EXPERIMENTAL PROCEDURE

As described in the previous section, the setup is simple in principle. There are three required elements: the film to be studied, the thermal imager, and a cold background source. For calibration, a monochromatic light source and an ordinary visible-light camera are also required. An overhead view of the arrangement used is given in Figure 5.

The infrared camera used in this experiment is an Inframetrics Model 600, built around a HgCdTe linear array detector cooled by liquid nitrogen and sensitive to long wave infrared (roughly 5-10  $\mu\text{m}$  wavelengths). Because few materials transmit light at these wavelengths, it uses no lenses but relies instead upon mirrors to provide the proper focus. A very rapidly rotating mirror scans the target area, shining one line at a time upon the detector. It is an old design made obsolete by focal-plane array (FPA) cameras, but it is sensitive enough and reasonably accurate to temperatures far below 277 K, with 237 to 257 K being the most useful range for our measurements. A photograph of the camera and its console is given in Figure 6.

Because the detector is cooled to liquid nitrogen temperatures, we may use a liquid nitrogen cooled background as well. A thin box was constructed for this purpose, with the faceplate of aluminum to facilitate rapid heat transfer and uniform temperatures, which was then covered by a thin uniform layer of black velvet to eliminate infrared reflections. This box was kept filled with liquid nitrogen at all times. It was placed well behind the film in order to keep convection from affecting the film and to keep the background out of focus, further increasing its uniform appearance.

Two frames are used in this experiment. The first is a simple rectangular frame suspended vertically, this used for the calibration procedure. The other is a pair of long rails, also vertical, fed by a reservoir at the top and forced to converge at the bottom. This convergence causes rapid draining and provides continuous flow. This device is our film tunnel, and it is used for all other experiments. A schematic of these and their dimensions is given in Figure 7.

Figure 8 shows a photograph of the apparatus from the perspective of the infrared camera. The rails of the film tunnel are visible in front of the blackbody. Figure 9 is a closeup of the tunnel in front of the background, showing the specific area examined. Figure 10 details the start of the film tunnel and the reservoir. Figure 11 shows the calibration frame in place.

In order to calibrate the setup, a monochromatic light source and an ordinary CCD camera are set to record the visible interference pattern on the film. We then hang the rectangular frame vertically and allow it to drain. In a few seconds, the film thickness describes a wedge-shaped profile, monotonically increasing towards the bottom. After enough time has passed, a black film is created at the top – the film has become so thin that there is no longer any liquid trapped between the layers of surfactant, but only the surfactant remains. Such a film uniformly reflects almost no visible light, and is therefore quite easy to identify. Its thickness can be computed mathematically and is less than the first-order fringe thickness. Since the thickness increases towards the bottom, the first bright fringe must be the first order fringe, followed by the second order fringe, and so on.

Infrared and visible images of the film are taken simultaneously. Given the wavelength of the visible light and the angle of incidence, each bright fringe gives us a point of known thickness to compare to the thermal image, and the relation between temperature and thickness can be determined.

Figures 12 and 13 show such an image pair. In Figure 12, the photograph is taken just prior to formation of the black film, and roughly twenty bright fringes are present. Figure 13 is the corresponding infrared image. Instead of an interference pattern, it shows a monotonically increasing temperature gradient towards the bottom. These images bear out the theory and provide us with an accurate relation between temperature and thickness.

After calibration, the film tunnel was used and images were taken of four separate cases. The first and simplest is the tunnel undisturbed. Second is the tunnel before being adjusted, showing separated boundary layers caused by small kinks in the rails. Next, a cylinder was inserted near one rail. Finally, a grid of cylinders was introduced in an effort to create grid turbulence.

## RESULTS

We begin by presenting the results of the calibration. The monochromatic light source used is a filtered mercury lamp, emitting green light at 546 nm and at an incident angle of 40.2 degrees. This produces a bright fringe spacing given by:

$$(28) \quad \frac{2\pi nh}{\lambda} \cos\theta = m \frac{\pi}{2} \quad m \text{ odd}$$

$$(29) \quad h = m 137.5 \text{ nm} \quad m \text{ odd}$$

Here the error in angle is estimated to be 1.0 degrees, giving an error of not more than 1.5%. This is not significant in the face of the uncertainty in aligning the images, although careful steps were taken there as well.

The calibration was performed several times, each with the camera adjusted to record a different temperature range. These data are presented in Figure 14, along with the theoretical curve and the least-squares straight line fit to the calibration data.

The calibration data is very linear in character, which was a bit of a surprise, but was not entirely unexpected in the face of the discussion. Apparently, simplifying the blackbody spectra to a single frequency is a very poor approximation, and the sine curve is blurred dramatically by the wide range of frequencies present. It is a pleasant surprise to see that the rough magnitude predicted by the theory is borne out by observation, but it was never the intent of the theory given above to provide a complete understanding, merely a line of reasoning to explain the phenomenon as a whole. In any event, the calibration data allows measurement of a wide range of film thickness as desired.

The best line fit to the calibration data is the following:

$$(30) \quad h = (82.60 \pm 2.35)T \frac{\mu\text{m}}{^{\circ}\text{C}} + (6920 \pm 210)\mu\text{m}$$

The positions of the fringes and the temperature boundaries were estimated using professional image enhancing software, but there remains uncertainty regarding the exact middle of the fringes and the average boundary between one temperature band and another. Errors in temperature are estimated at one-half of one division, or 1.25 K to 2.5 K depending on the calibration run. Error in thickness is uniformly estimated at one-quarter the fringe spacing, or 70 nm. But taken in total, this is quite accurate. The film thickness observed in the film tunnel typically ranged from 3600 nm to 5300 nm, giving us a total accuracy of 10% overall or better for these measurements.

The infrared images provided by the Inframetrics 600 camera are 128x128 pixels at 30 Hz with 20 steps of temperature resolution. These are captured onto video disc and digitized for processing. All images presented have been de-interlaced to correct color errors produced by the capture system.

Figure 15 is an infrared image of the film tunnel operating at its best. The temperature ranges from -40 to -20 degrees Celsius in 2.5 degree steps. The bright lines on either side of the image are the rails of the tunnel spaced 4 cm apart. This image provides us with an estimate of the overall system accuracy.

Figure 16 shows the same area of the tunnel prior to its final adjustment. We can clearly see the thinner regions at both sides where the flow has separated. Outside these regions the thickness of the film has not changed.



Figure 17 was taken with a 1.5 mm cylinder held at the wall just upstream of the infrared image. The cylinder was not included in the image to keep extraneous infrared light emitted by the cylinder (and the hand holding it) from affecting the image. Here the temperature range has been adjusted, now between -36.6 and -26.6 degrees Celsius. We can plainly see the wake of the cylinder growing behind it and can possibly resolve some of the wake structure as well.

In Figure 18 we have the same scenario as in Figure 17, except now we are looking at a much larger section of the tunnel at a penalty in resolution.

Figure 19 is a picture of the grid used to generate grid turbulence. The grid measures 3.5 cm wide and has 15 cylinders evenly spaced each 1.5 mm across. Figure 20 is an infrared image of the flow shortly after the introduction of the grid. The temperature range here is -40 to -20 degrees Celsius.

Figures 15, 16, 17, and 20 are all presented here in processed form. The images were first converted to a higher resolution, then passed through de-noising and averaging filters, giving the effect of color correction and a 2x2 smoothing upon the original image. The resulting graphs have all been forced to a uniform color map and calibrated to give the film thickness. These graphs are given in Figures 21 through 24. In each of these figures the color map reads from 3.6  $\mu\text{m}$  to 5.3  $\mu\text{m}$  in 20 even steps of 0.9  $\mu\text{m}$  each. It should be pointed out that the actual rail temperature is much higher than the readings given in these figures; it is simply off of the scale.

The unobstructed flow examples are by themselves sufficiently clear, and no new detail is uncovered in the processed images. These serve only to clarify the thickness computation and display the film thickness in an intuitive format. The cylinder wake, on the other hand, is considerably cleaner and a number of vortex cores may be showing within, although they are rather faint. This wake appears exactly as one would expect. It is worth mentioning that the live video itself seems to contain more detail than the sum of its stills, likely because the evolution of one structure into another then becomes clearer. To illustrate this, in Figure 25 two consecutive raw infrared images, taken of the cylinder wake, are placed side by side. The change between the first and the second is not very great, allowing the inner details of both to be considered. This effect is amplified as more images are available.

Figure 24 provides a good deal of detail with regard to the flow behind the grid. A number of fairly strong vortices are close to the left rail, and perhaps a few weaker ones at right. Unfortunately, this does not appear to be grid turbulence, as these are the only obvious structures present. The grid seems instead to be blocking the tunnel, except for a gap at the left side which is then shedding the strong vortices. If grid turbulence is indeed being created, it is all but lost in the rough surface of the film. A more suitable grid and possibly more thickness resolution appear to be needed here.

## DISCUSSION

The discrepancies between the theoretical calibration curve and the measured curve are significant and perhaps could be harnessed to better define the theory. The two unresolved questions are:

1. How does the blackbody spectrum, especially corrected for camera response, affect the calculation? And:
2. What is the energy contribution from the film itself, and is this reflected, or emitted, or both?

The first question may be solvable mathematically. It would prove interesting to perform a numerical integral of the energy flux terms over the range of frequencies detected by the camera. We suspect the new theoretical relation between thickness and temperature would prove to be more linear and less sinusoidal, but this is not obvious.

Calculating the emittance of the film analytically appears extremely difficult. It is not clear how an object radiates for thickness  $h \ll \lambda$ , and how the camera and the rest of the laboratory reflect back to the camera is very complicated. Answering this question would seem to be simpler from an experimental standpoint. With a more responsive camera, one could reduce the background temperature even further, until the film term completely dominates the energy balance. By tracking the calibration for decreasing  $T_{bg}$ , it should be possible to arrive at a reasonable estimate of the film emittance.

Arriving at the thickness measurement of the film has proven to be very simple once the calibration is complete, and the pressure relates to the thickness linearly. Calculation of the velocity profile can also be performed, although this process is more involved. Given a start condition of known velocity, for instance a uniform velocity field in the film tunnel, one can compute the evolution of the velocity field over time, by applying the Reynolds equation (equations (5) through (9) ) to successive frames.

Another obvious method for velocity calculation, one for which this method seem uniquely suited, would be the application of image correlation velocimetry (ICV). Since thickness is an advected scalar, it is an appropriate quantity for ICV, and many images may be obtained very cheaply. This is especially attractive because it requires no modifications to the experiment, but only more computation.

Comparison between the calibration images for visible and infrared light reveal that the information provided by this method is comparable to that of simple interferometry, but that the level of detail is not as good. This is not true in general. The infrared method is limited in resolution only by the sensitivity of the camera and the uniformity of the infrared background, whereas the resolution of interference methods is limited by the fringe spacing.

The resolution of this system appears to be sufficient for calculation of fluid properties and is suitable for examining cylinder wakes and like problems, but does not appear to be enough for more detailed studies, such as grid turbulence. This can be remedied using more powerful imagers. At the time of writing the state-of-the-art cameras employ a 2,000x2,000 liquid nitrogen cooled detector, capable of resolving temperature differences as small as 0.1 K at 150 K reported temperature, at scan rates of 120 Hz or more. This represents an improvement in sensitivity of roughly four orders of magnitude over the equipment used in this study. Other improvements can be made to the infrared background and the film itself, both of which would be necessary to take full advantage of such a device.

## CONCLUSIONS

The method presented here offers a completely new way to study soap film flows, affording a non-intrusive and relatively simple process to globally measure the thickness of the film, which is in general not obtainable by other methods. This information is useful in calculating the other properties of the flow as well, in particular the pressure, and is a key part of the velocity computation. While all of the mechanics of the method are not fully understood, this is not necessary for application. At present, a basic model is given, and new questions and shortcomings are identified.

Pending resolution of the physical behavior, an easy calibration routine is included, which is demonstrated to provide usable accuracy and is at the least supported by the basic model. Using very average equipment, this study achieved thickness measurements with better than 10% accuracy from 1.8  $\mu\text{m}$  to 6.5  $\mu\text{m}$  and more, bracketing the most useful range 3.6  $\mu\text{m}$  to 5.3  $\mu\text{m}$ .

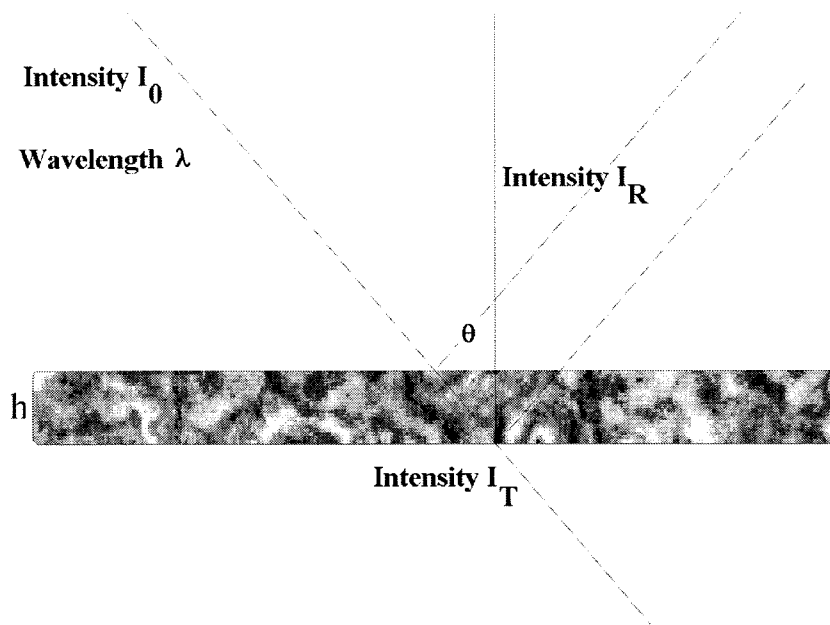
The infrared method and the calibration are then applied to a few typical problems of thin film flow. As with interference imaging this is best applied to a film with flat geometry, such as the film tunnel. In all cases the data gathered proved to be at least competitive with the detail available from other methods, and shows the potential to improve upon all others.

Finally, some preliminary forays into calculations using the pressure data were discussed, and processed images of the thickness are given. From these one can begin further calculation, integrating over time to find velocity or applying other methods, such as ICV, to determine the velocity field and therefore the total state of the system.

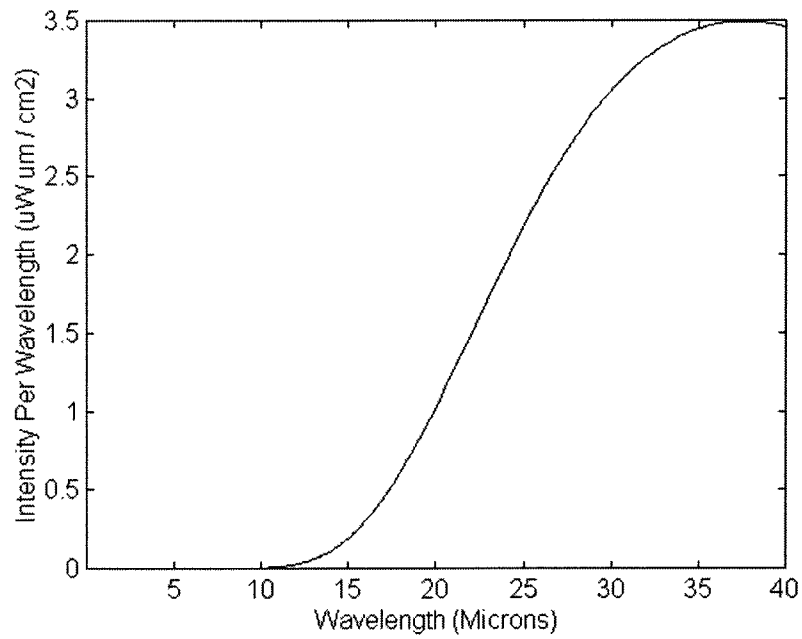
It is hoped that, with this method and its capabilities, soap film flows and two-dimensional problems in general will become better understood and more applicable to other areas of fluid mechanics.

## BIBLIOGRAPHY

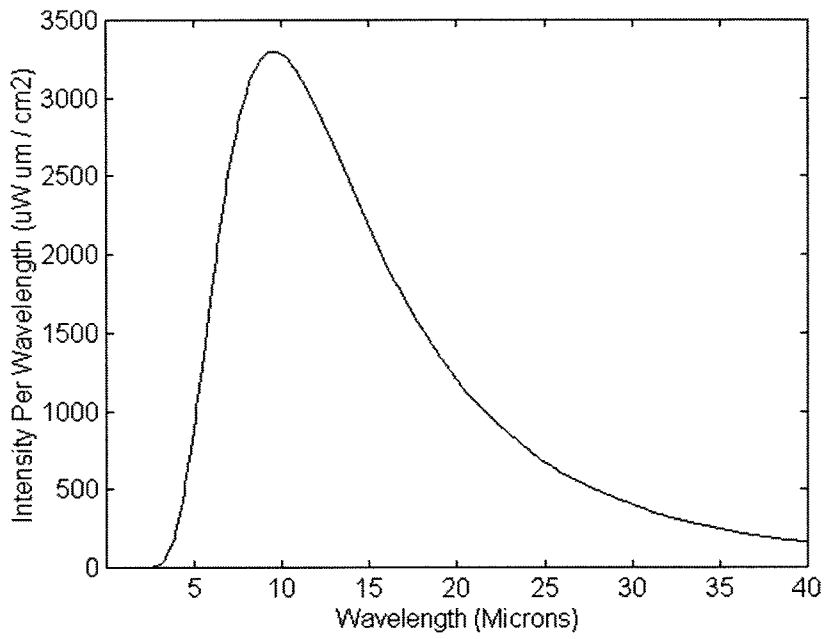
1. "On the Hydrodynamics of Soap Films," Y. Couder, J. Chomaz, M. Rabaud, *Physica D*, v37, pp.364-405, 1989
2. "A Liquid Film (Soap Film) Tunnel to Study Two Dimensional Laminar and Turbulent Shear Flows," M.Gharib, P. Derango. *Physica D*, v37, pp. 406-416, 1989
3. "Soap Films as Two Dimensional Classical Fluids," J. Chomaz, B. Cathalau. *Physical Review A* v41, pp. 2243-2245, 1990
4. Soap Films: Studies of Their Thinning and a Bibliography, K Mysels, K Shinoda, S. Frankel. Pergamon Press, 1959
5. "Shear Flow in a Two Dimensional Couette Cell: A Technique for Measuring the Viscosity of Free-Standing Liquid Films," B. Martin, X-L. Wu., 1995



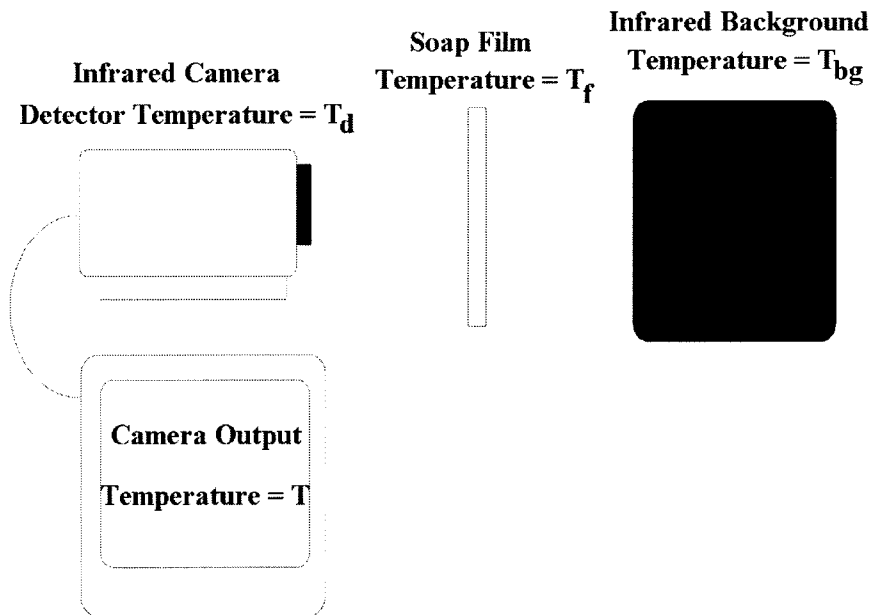
**Figure 1: Thin Film Interference**



**Figure 2: Blackbody Spectrum at 77K**

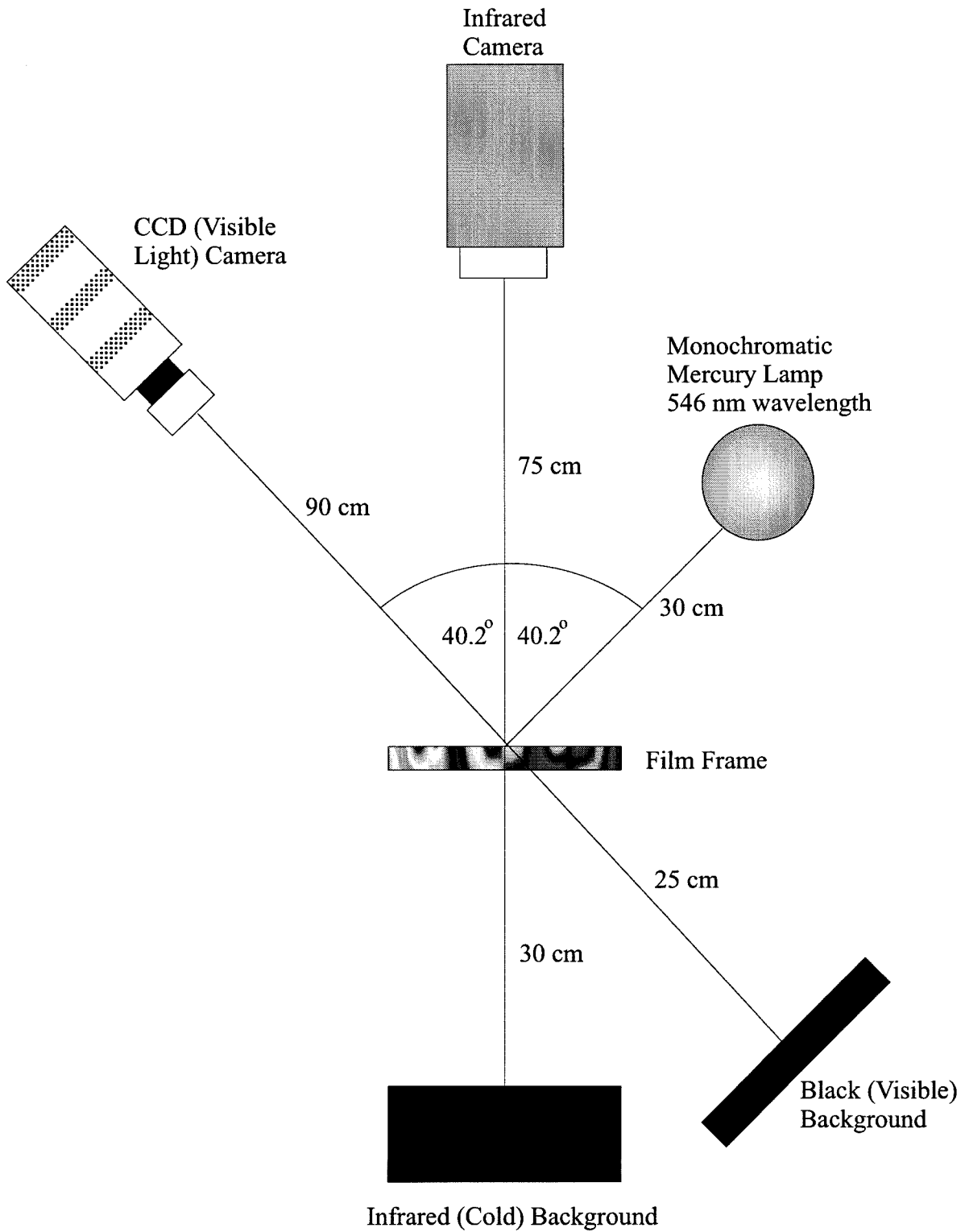


**Figure 3: Blackbody Spectrum at 303 K**



**Figure 4: Basic Setup**

Figure 5: Top View and Dimensions of Setup



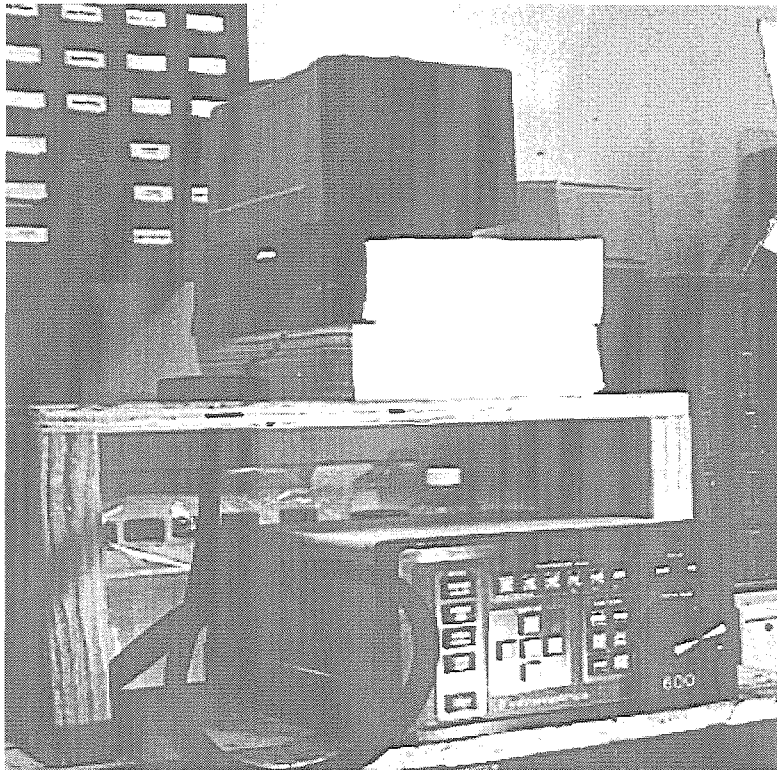
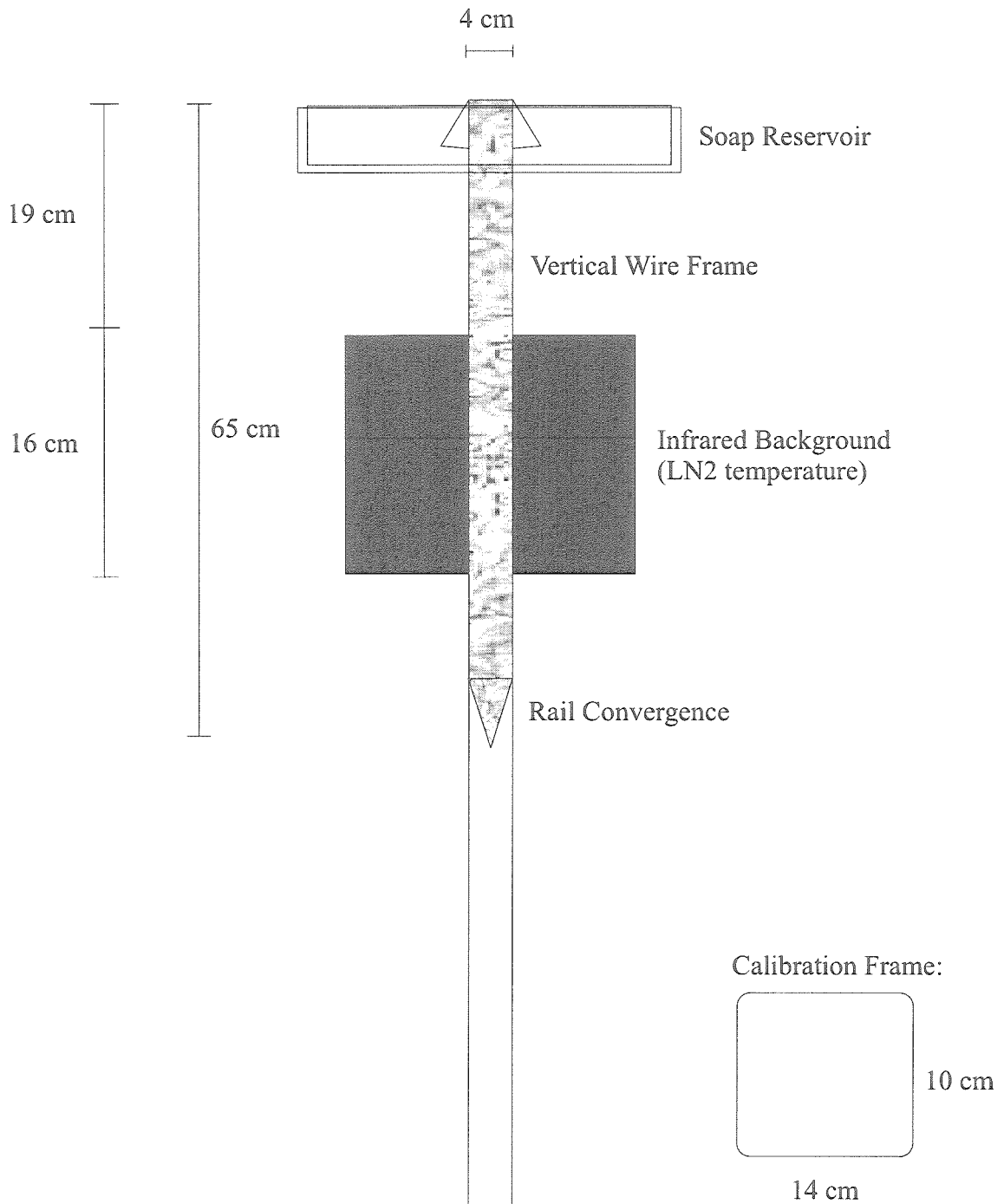


Figure 6: Infrared Camera and Console



Figure 7: Configuration and Dimensions of Film Tunnel



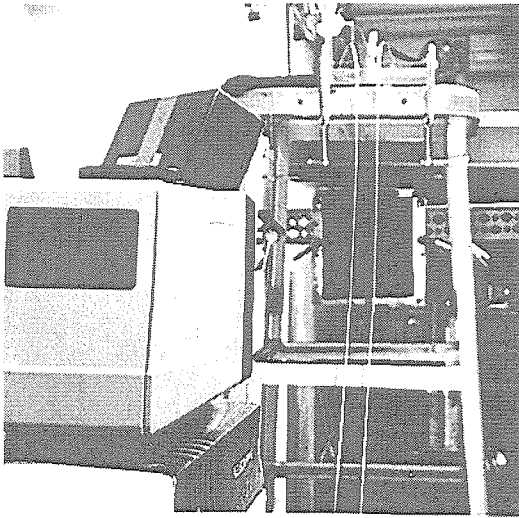


Figure 8: Looking Past the IR Camera

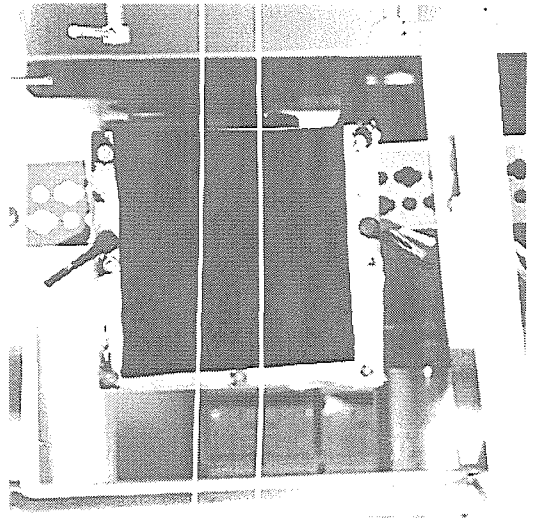


Figure 9: Closeup of the Film Tunnel Rails

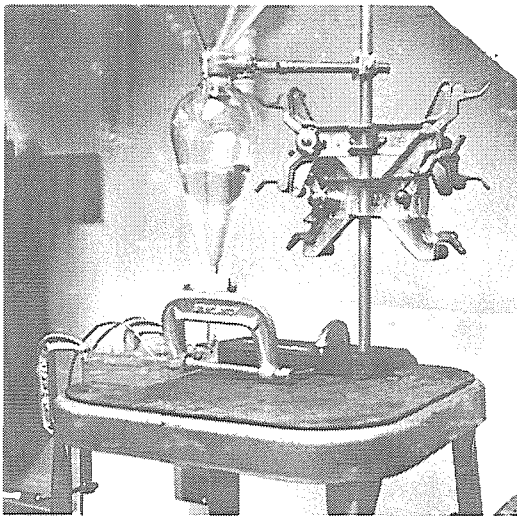


Figure 10: Film Tunnel Reservoir

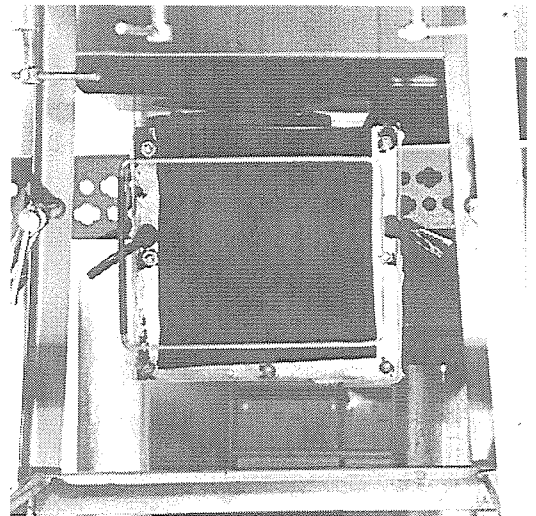
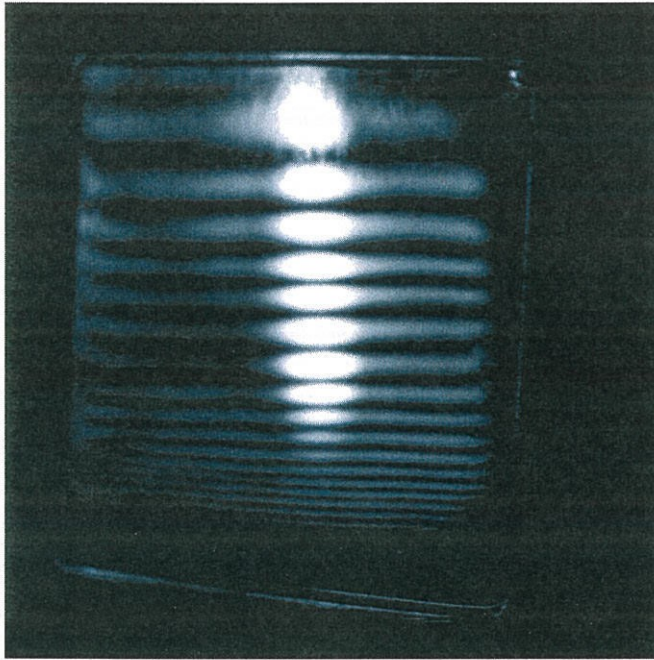
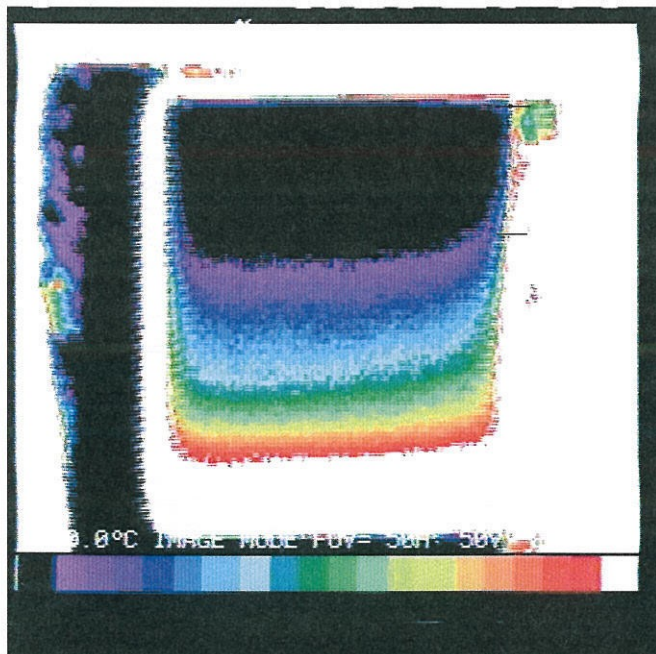


Figure 11: Calibration Frame



**Figure 12: Calibration Interference Image**



**Figure 13: Infrared Calibration Image**

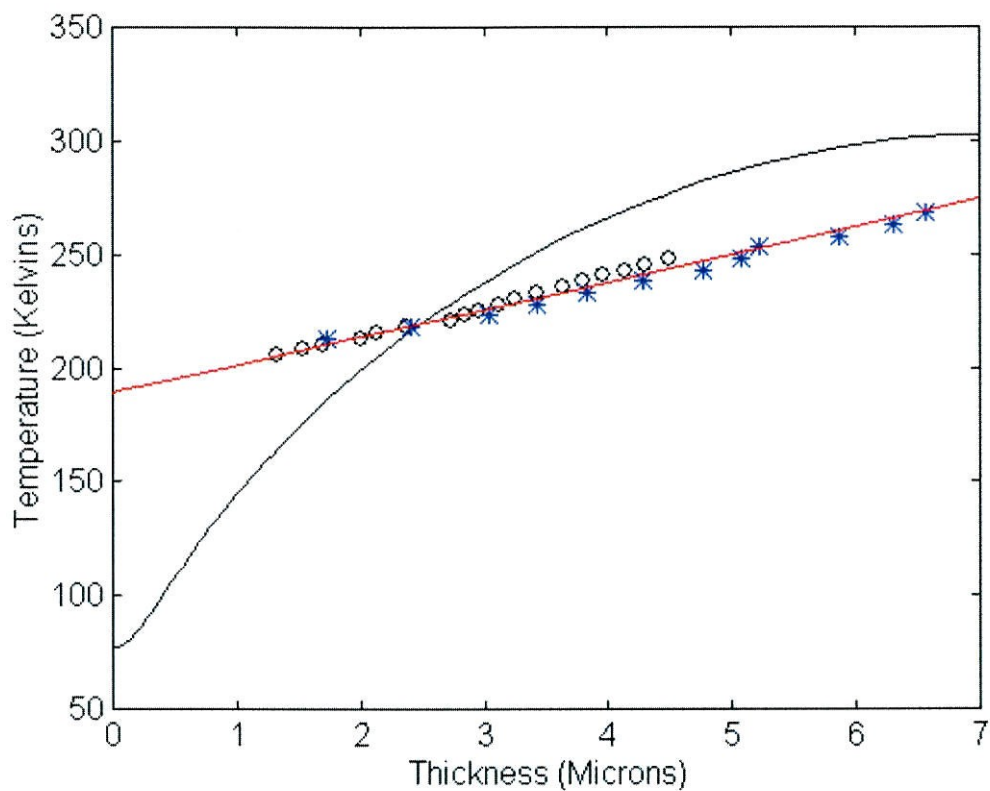


**Figure 14: Calibration Data**  
**Red Line -- Best Linear Fit**  
**Black Curve -- Theoretical Prediction**

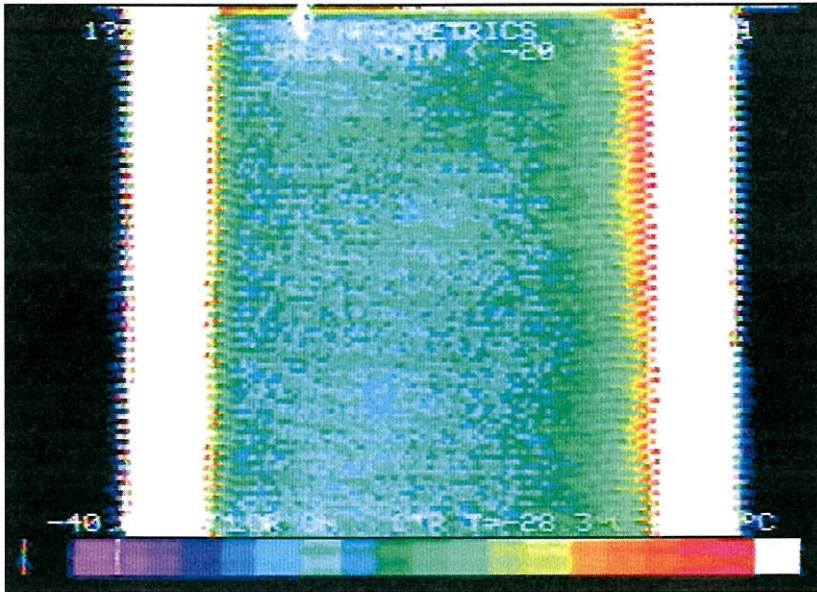


Figure 15: Raw Infrared Image of Undisturbed Film Tunnel Flow

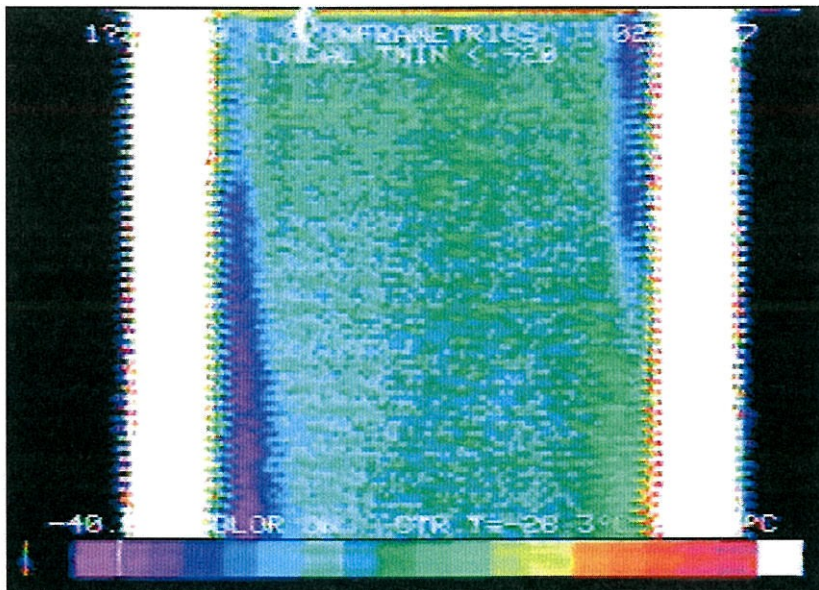


Figure 16: Raw Infrared Image of Separated Tunnel Flow

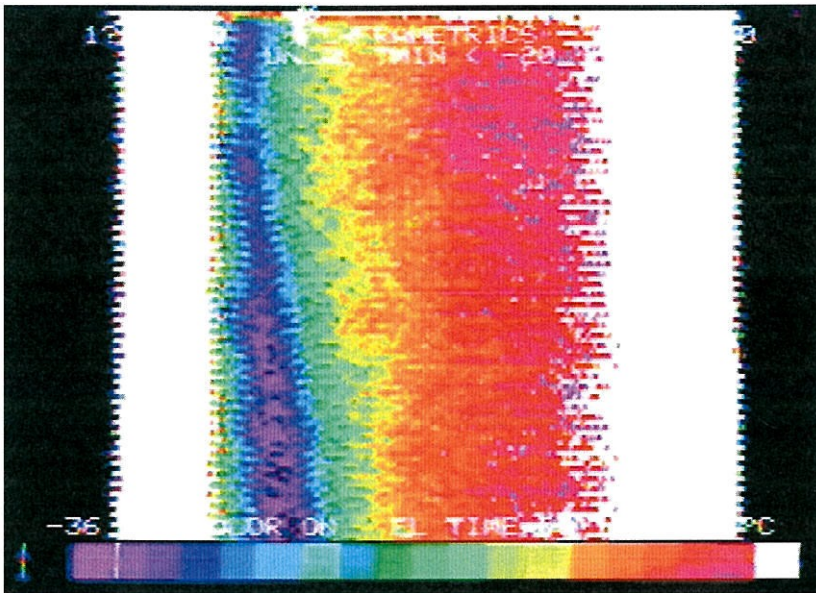


Figure 17: Wake Behind a Cylinder

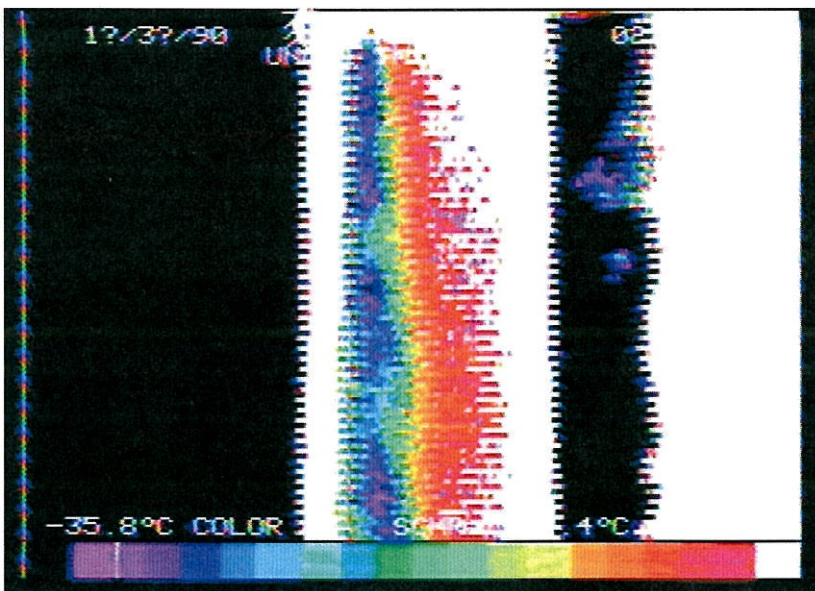


Figure 18: Wake Behind a Cylinder

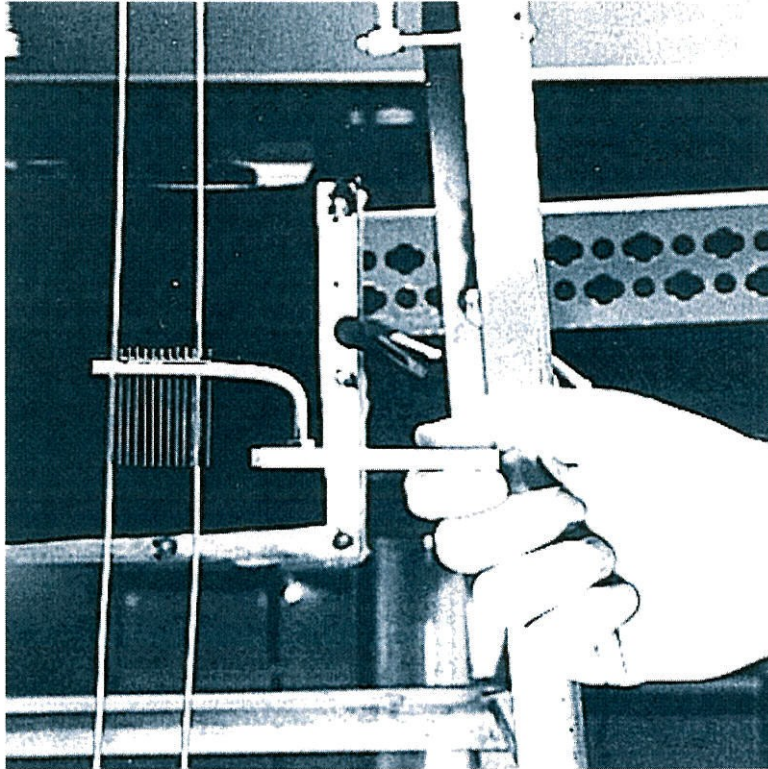


Figure 19: The Grid

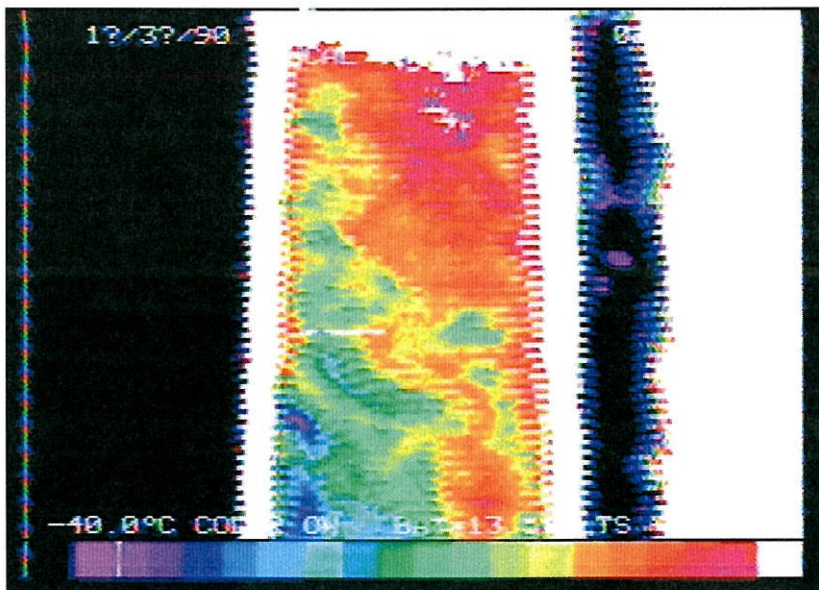
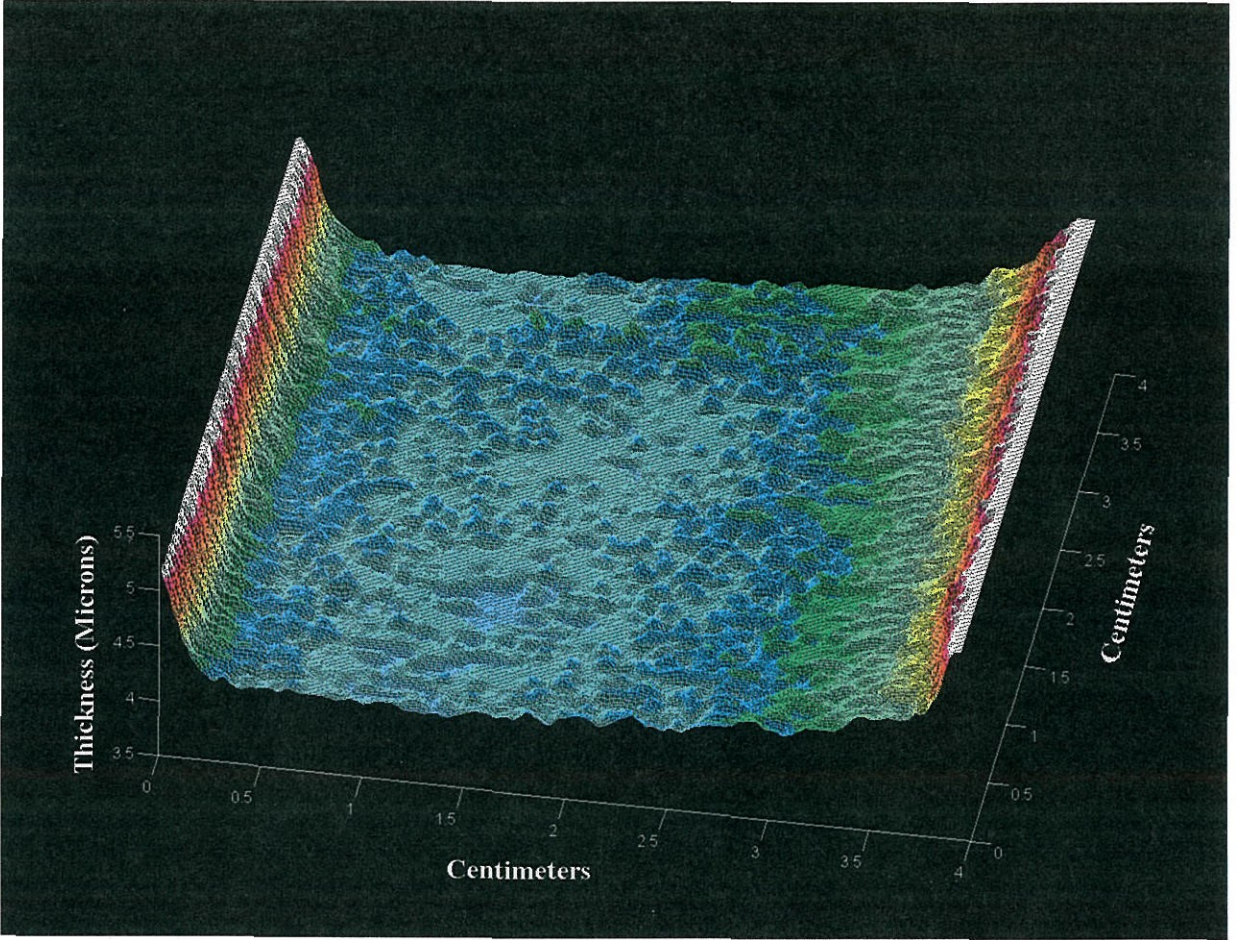
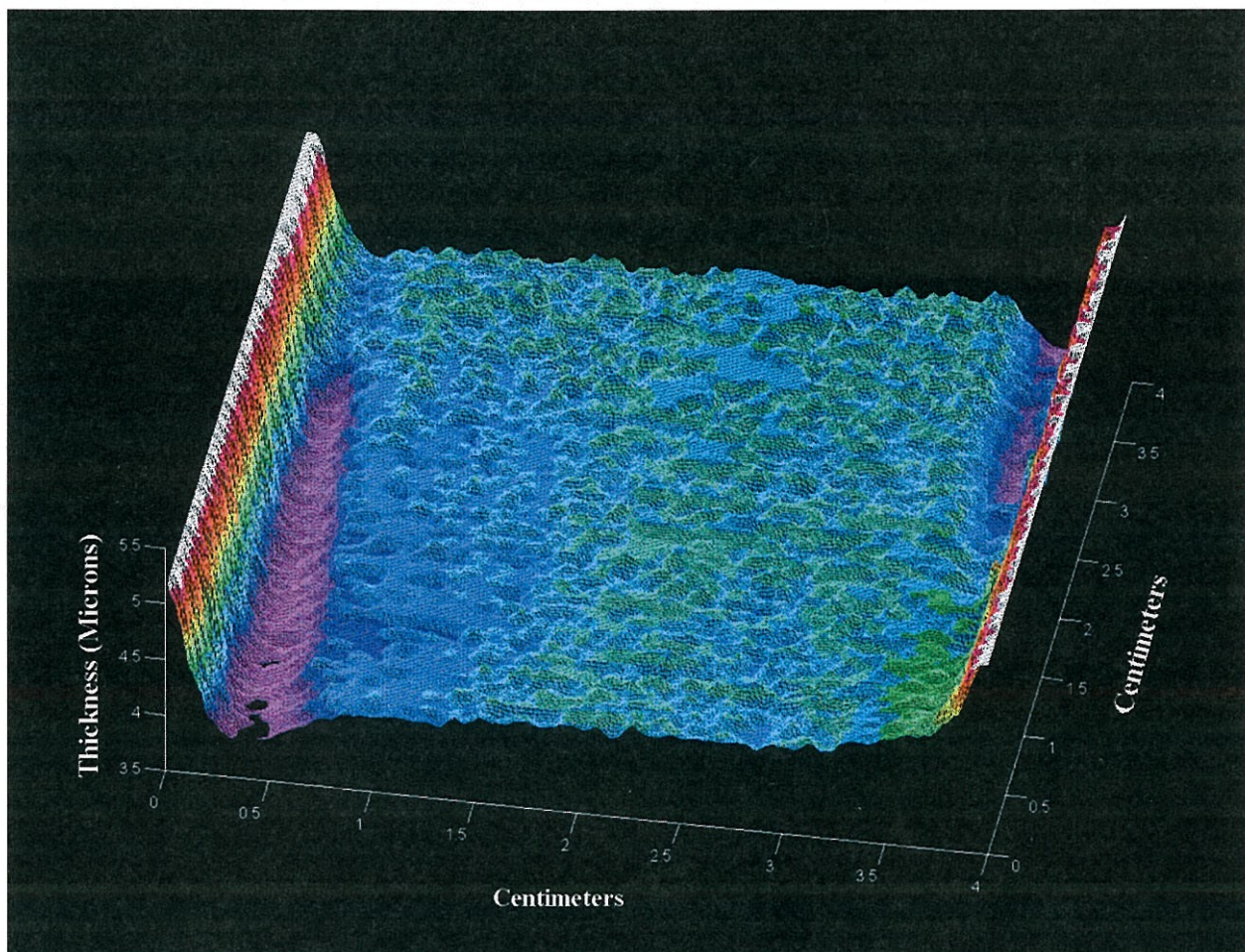


Figure 20: Raw Infrared Image of Flow Behind the Grid



**Figure 21: Processed Infrared Image  
Undisturbed Tunnel Flow Film Thickness**





**Figure 22: Processed Infrared Image  
Separated Tunnel Flow  
Film Thickness Plot**

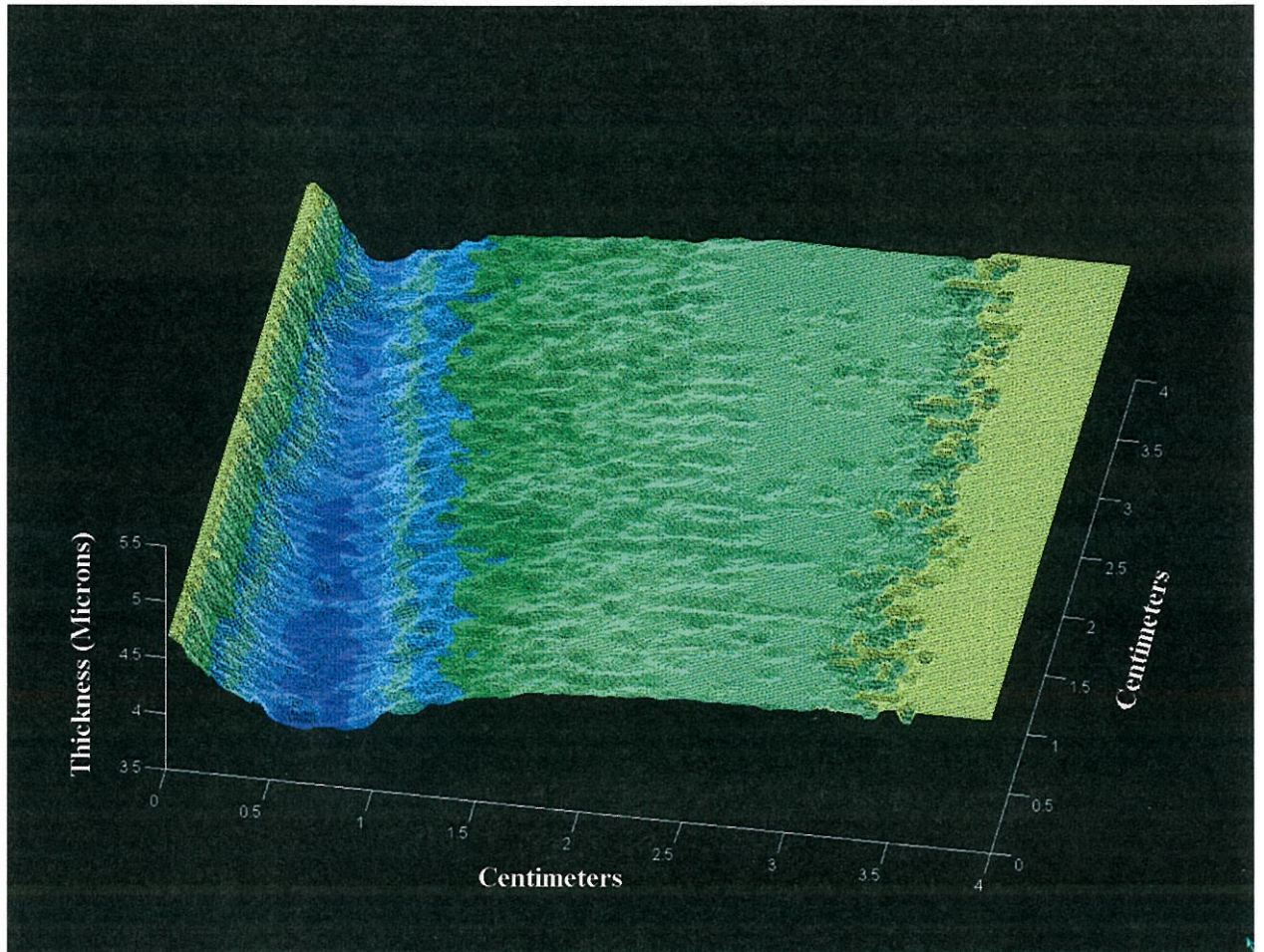


**Figure 23: Processed Infrared Image  
Wake Behind Cylinder in Film Tunnel  
Film Thickness Plot**

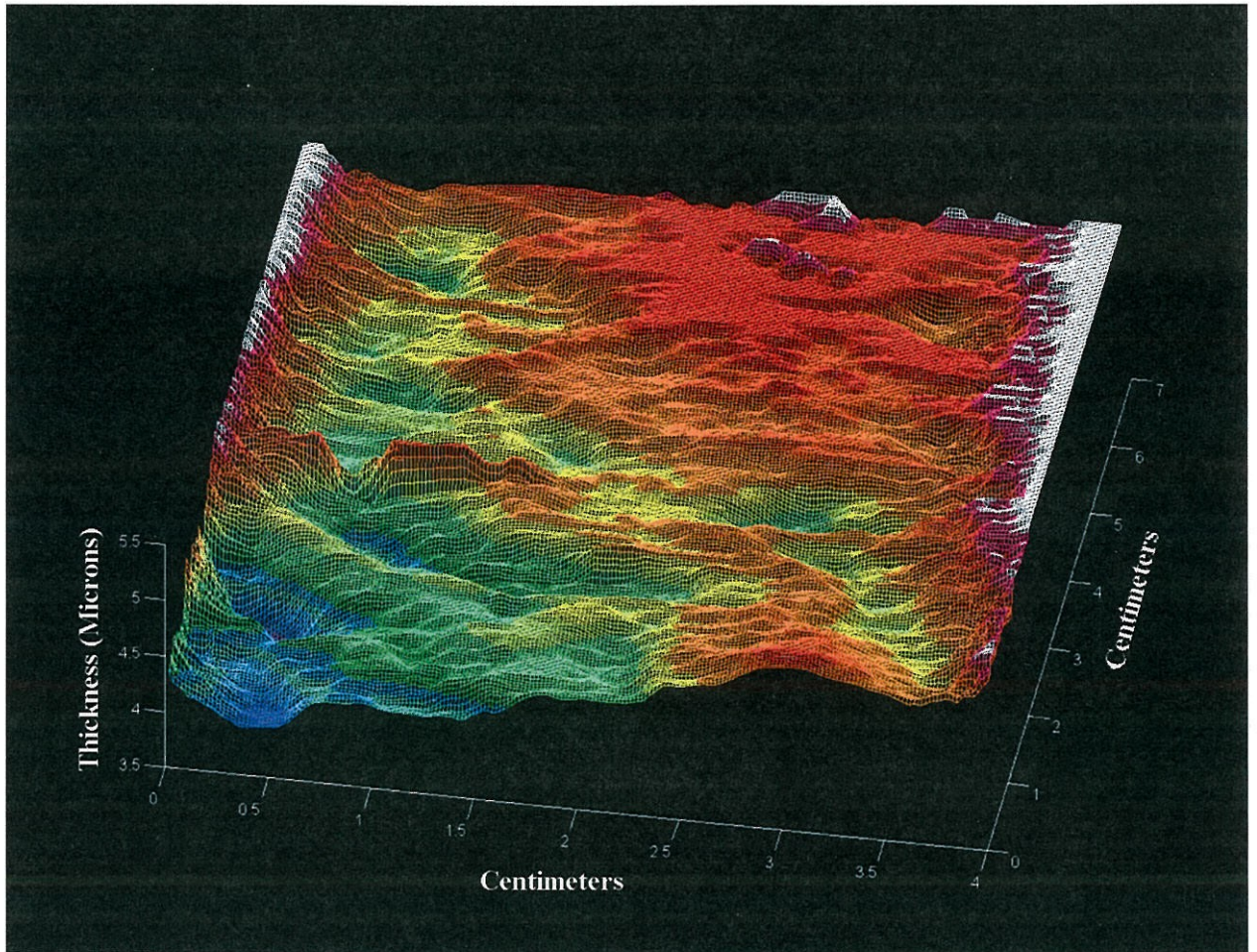


**Figure 24: Processed Infrared Image  
Film Tunnel Flow Past the Grid  
Film Thickness Plot**

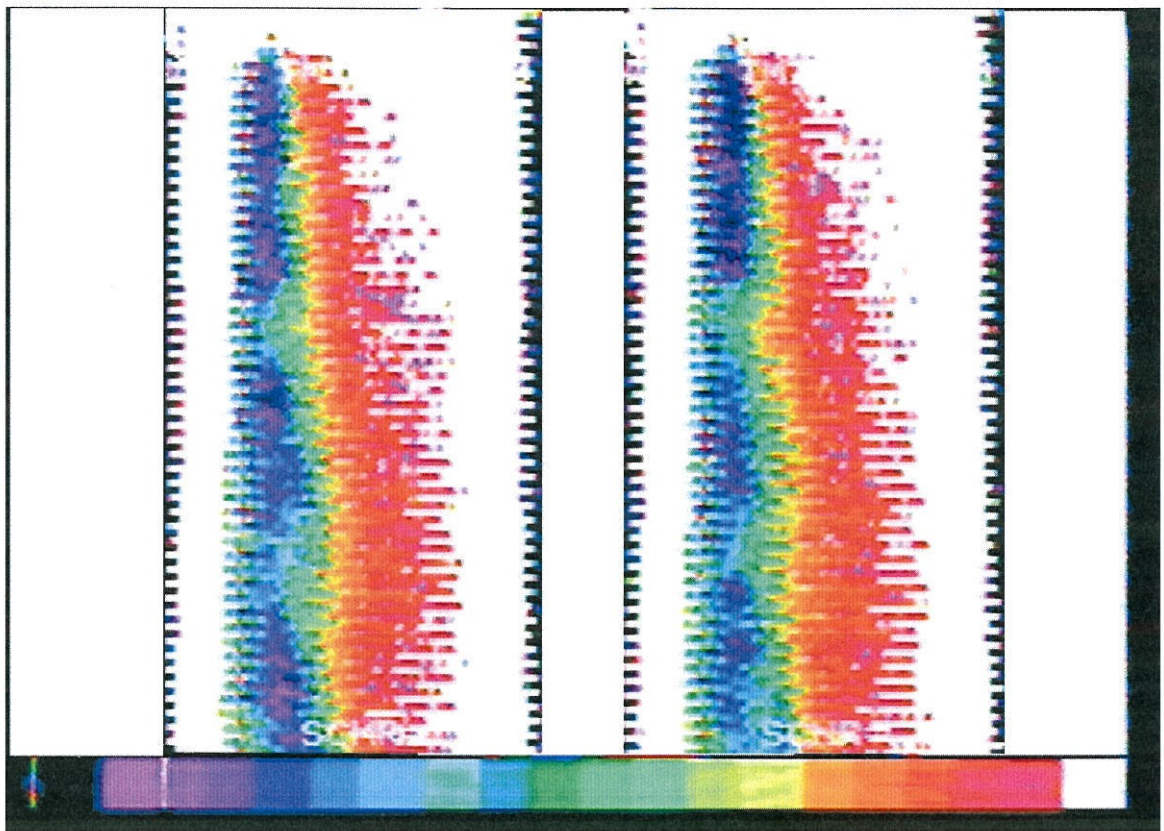


Figure 25: Two Subsequent Raw Infrared Images  
Separated Flow Past a Cylinder  
Time Interval = 1/30 second